Correction for fast pseudo-diffusive fluid motion contaminations in diffusion tensor imaging

Stieb, Sonja ; Klarhoefer, Markus ; Finkenstaedt, Tim ; Wurnig, Moritz C ; Becker, Anton S ; Rossi, Cristina

Abstract: In this prospective study, we quantified the fast pseudo-diffusion contamination by blood perfusion or cerebrospinal fluid (CSF) intravoxel incoherent movements on the measurement of the diffusion tensor metrics in healthy brain tissue. Diffusion-weighted imaging (TR/TE = 4100 ms/90 ms; b-values: 0, 5, 10, 20, 35, 55, 80, 110, 150, 200, 300, 500, 750, 1000, 1300 s/mm2, 20 diffusion-encoding directions) was performed on a cohort of five healthy volunteers at 3 Tesla. The projections of the diffusion tensor along each diffusion-encoding direction were computed using a two b-value approach (2b), by fitting the signal to a monoexponential curve (mono), and by correcting for fast pseudo-diffusion compartments using the biexponential intravoxel incoherent motion model (IVIM) (bi). Fractional Anisotropy (FA) and Mean Diffusivity (MD) of the diffusion tensor were quantified in regions of interest drawn over white matter areas, gray matter areas, and the ventricles. A significant dependence of the MD from the evaluation method was found in all selected regions. A lower MD was computed when accounting for the fast-diffusion compartments. A larger dependence was found in the nucleus caudatus (bi: median 0.86 10-3 mm2/s, Δ2b: -11.2%, Δmono: -14.4%; p = 0.007), in the anterior horn (bi: median 2.04 10-3 mm2/s, Δ2b: -9.4%, Δmono: -11.5%, p = 0.007) and in the posterior horn of the lateral ventricles (bi: median 2.47 10-3 mm2/s, Δ2b: -5.5%, Δmono: -11.7%; p = 0.007). Also for the FA, the signal modeling affected the computation of the anisotropy metrics. The deviation depended on the evaluated region with significant differences mainly in the nucleus caudatus (bi: median 0.15, Δ2b: +39.3%, Δmono: +14.7%; p = 0.022) and putamen (bi: median 0.19, Δ2b: +3.1%, Δmono: +17.3%; p = 0.015). Fast pseudo-diffusive regimes locally affect diffusion tensor imaging (DTI) metrics in the brain. Here, we propose the use of an IVIM-based method for correction of signal contaminations through CSF or perfusion.

DOI: https://doi.org/10.1016/j.mri.2019.09.009

Stieb, Sonja; Klarhoefer, Markus; Finkenstaedt, Tim; Wurnig, Moritz C; Becker, Anton S; Rossi, Cristina (2020). Correction for fast pseudo-diffusive fluid motion contaminations in diffusion tensor imaging. Magnetic Resonance Imaging, 66:50-56.
DOI: https://doi.org/10.1016/j.mri.2019.09.009

Journal Pre-proof

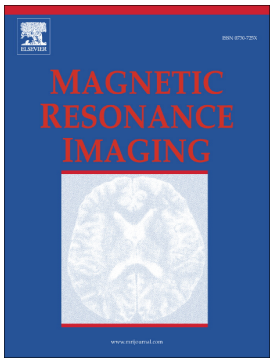

Correction for fast pseudo-diffusive fluid motion contaminations in diffusion tensor imaging

Sonja Stieb, Markus Klarhoefer, Tim Finkenstaedt, Moritz C. Wurnig, Anton S. Becker, Cristina Rossi

PII: S0730-725X(19)30267-X

DOI: https://doi.org/10.1016/j.mri.2019.09.009

Reference: MRI 9318

To appear in: *Magnetic Resonance Imaging*

Received date: 29 April 2019

Revised date: 18 July 2019

Accepted date: 15 September 2019

Please cite this article as: S. Stieb, M. Klarhoefer, T. Finkenstaedt, et al., Correction for fast pseudo-diffusive fluid motion contaminations in diffusion tensor imaging, *Magnetic Resonance Imaging*(2018), https://doi.org/10.1016/j.mri.2019.09.009

MANUSCRIPT

Correction for Fast Pseudo-diffusive Fluid Motion Contaminations in Diffusion Tensor Imaging

Sonja Stieb, MD[a], Markus Klarhoefer, PhD[b], Tim Finkenstaedt, MD[a], Moritz C. Wurnig, MD[a], Anton S. Becker, MD[a], Cristina Rossi, PhD[a]

[a]Institute of Diagnostic and Interventional Radiology, University Hospital Zurich, University of Zurich, Switzerland

[b]Siemens Healthcare AG, Zurich, Switzerland

Declarations of interest: Dr. Klarhoefer is employed by Siemens Healthcare. He was mainly involved in MRI protocol optimization.

Corresponding author

Sonja Stieb, MD

Department of Radiation Oncology

The University of Texas MD Anderson Cancer Center

1515 Holcombe Blvd

Houston, Texas 77030

United States of America

Phone: +1 713 745 8273

Email: smstieb@mdanderson.org

ABSTRACT

In this prospective study, we quantified the fast pseudo-diffusion contamination by blood perfusion or cerebrospinal fluid (CSF) intravoxel incoherent movements on the measurement of the diffusion tensor metrics in healthy brain tissue.

Diffusion-weighted imaging (TR/TE = 4100 ms/ 90 ms; b-values: 0, 5, 10, 20, 35, 55, 80, 110, 150, 200, 300, 500, 750, 1000, 1300 s/mm^2, 20 diffusion-encoding directions) was performed on a cohort of five healthy volunteers at 3 Tesla. The projections of the diffusion tensor along each diffusion-encoding direction were computed using a two b-value approach (2b), by fitting the signal to a monoexponential curve (mono), and by correcting for fast pseudo-diffusion compartments using the biexponential intravoxel incoherent motion model (IVIM) (bi). Fractional Anisotropy (FA) and Mean Diffusivity (MD) of the diffusion tensor were quantified in regions of interest drawn over white matter areas, gray matter areas, and the ventricles.

A significant dependence of the MD from the evaluation method was found in all selected regions. A lower MD was computed when accounting for the fast-diffusion compartments. A larger dependence was found in the nucleus caudatus (bi: median 0.86 10^{-3} mm^2/s, Δ2b: -11.2%, Δmono: -14.4%; p=0.007), in the anterior horn (bi: median 2.04 10^{-3} mm^2/s, Δ2b: -9.4%, Δmono: -11.5%, p=0.007) and in the posterior horn of the lateral ventricles (bi: median 2.47 10^{-3} mm^2/s, Δ2b: -5.5%, Δmono: -11.7%; p=0.007). Also for the FA, the signal modelling affected the computation of the anisotropy metrics. The deviation depended on the evaluated region with significant differences mainly in the nucleus caudatus (bi: median 0.15, Δ2b: +39.3%, Δmono: +14.7%; p=0.022) and putamen (bi: median 0.19, Δ2b: +3.1%, Δmono: +17.3%; p=0.015).

Fast pseudo-diffusive regimes locally affect diffusion tensor imaging (DTI) metrics in the brain. Here, we propose the use of an IVIM-based method for correction of signal contaminations through CSF or perfusion.

1. Introduction

Diffusion-weighted imaging (DWI) has a broad spectrum of applications in neuroradiology (1). DWI is used in the detection of cerebral ischemia (2), in the grading of tumors (3), in the detection and

differentiation of infections (4), and in the analysis of structural changes in neurodegenerative diseases (5).

Especially for white matter diseases, the diffusion tensor imaging (DTI), an advanced acquisition strategy and post-processing data evaluation of DW-images, gives additional information. By assessing the main diffusion vectors in each voxel, the fractional anisotropy (FA) and the mean diffusivity (MD) can be calculated to allow conclusions about the integrity of fibers and the potential restriction of the water diffusion in the voxel.

In the clinical routine, echo-planar imaging (EPI) readout combined with two b-values is mainly used for DWI acquisitions. However, the potential contribution of fast-pseudo diffusion compartments is not accounted for. The intravoxel incoherent motion imaging (IVIM) was, therefore, proposed by Le Bihan et al. (6). The observed signal pattern deviations from the monoexponential decay, predicted from the assumption of a Gaussian diffusion regime, were attributed to the effect of blood perfusion. The group suggested that the signal decay could be more precisely described with a biexponential curve. In the brain, the first part of the curve, from b-value 0 s/mm^2 to approximately 200 s/mm^2, shows a rapid decay and is mainly attributed to blood perfusion in randomly distributed capillary segments within the voxel. The second part (for b-values up to 1000 s/mm^2) is mostly dominated by the thermal-driven diffusion of the water molecules in the extracellular space.

Not only perfusion but also other sources of intravoxel incoherent water motion result in a pseudo-diffusive regime (7). In areas of larger contamination of the cerebrospinal fluid (CSF), a significant inaccuracy of the diffusion tensor metrics is expected (8). Several methods have been proposed in the past to correct for those effects (e.g., FLAIR DWI (9), or free water elimination (10)). Relevant to the topic of this study are the methods based on the intravoxel signal modeling published by Metzler-Baddeley et al. (11). With their voxel-by-voxel free-water elimination approach by using two b-values, a significant increase in FA and a decrease in MD was found compared to the uncorrected values in areas of expected CSF contamination (11). In this study, we propose the use of biexponential modeling of the DW-signal acquired using multiple b-values for post-processing correction of fast pseudo-diffusion contaminations on the estimation of the diffusion tensor metrics in the brain.

2. Material and Methods

The prospective study took place at XXX (blinded for review). The study had been approved by the local ethics committee (No. XXX, blinded for review) and was performed in accordance with the Declaration of Helsinki. The study was part of a larger ongoing study where the influence of examination time on patient comfort during an MRI exam was evaluated.

2.1 Participants

Five healthy volunteers have been included in this study (all male, 25 - 64 years old, mean: 36 years). All participants gave written informed consent to the examination and the scientific evaluation of the data.

2.2 Study protocol

The study MRI was acquired on a 3 Tesla whole-body scanner (MAGNETOM Skyra, Siemens Healthcare, Erlangen, Germany). A 64-channel head coil was used for signal acquisition, and a body transmit coil for spin excitation.

First, a 3D T1-weigthed Magnetization-Prepared Rapid Gradient-Echo (MPRAGE) sequence was acquired for anatomical orientation (TR=7 ms, TE=2.32 ms, TI=900ms, flip angle=8°, GRAPPA acceleration factor 2). Then, a fat-saturated diffusion-weighted Echo Planar Imaging (EPI) sequence was acquired over 30 minutes (TR=4100 ms; TE=90 ms; echo spacing=0.68 ms; readout bandwidth 1685 Hz/px, GRAPPA acceleration factor 2; partial Fourier 7/8; voxel size 2×2×2 mm^3; b-values: 0, 5, 10, 20, 35, 55, 80, 110, 150, 200, 300, 500, 750, 1000, 0, 110, 150, 200, 300, 500, 750, 1000, 0, 0 s/mm^2, 20 diffusion-encoding directions, 24 slices).

2.3 Post-processing

Before computation of the parametrical maps, diffusion-weighted volumes were realigned to the first b0-volume using the “diffusion” toolbox of SPM 12 (Statistical Parametrical Mapping 12, Wellcome Trust Centre for Neuroimaging, London, UK). The T1-weighted volume was coregistered to the b0-volume using SPM.

For each diffusion-encoding direction, the projections of the diffusion tensor were computed from the DW-signals measured over regions of interest (ROIs) described below using three different frameworks. The MR images were processed off-line using in-house custom software that was written in Matlab (MATLAB Release 2016b, The MathWorks, Inc., Natick, Massachusetts, USA):

a) Signal attenuation at b=1000 s/mm^2

   In this case, a Gaussian diffusion regime was assumed, and the projection of the diffusion tensor along the diffusion-encoding direction (D_i) was computed from the equation:

$$D_i = \frac{lnS_b - ln\ S_0}{b_i} \quad [1]$$

b) Monoexponential fitting

As in the previous case, also here a Gaussian diffusion regime was assumed. The projection of the diffusion-tensor along the gradient direction was computed by fitting the signal acquired for the different b-values to the equation, using a Levenberg-Marquardt algorithm:

$$S_{b,i} = S_0 + e^{-b_i \cdot D_i} \quad [2]$$

c) Biexponential fitting

In this third scenario, a biexponential signal attenuation was assumed. The projections of the diffusion tensor along the single diffusion-encoding directions were estimated after correction for the presence of a fast pseudo-diffusion compartment as described by Wurnig and colleagues (12). The algorithm is based on an iterative two-step fitting approach separating, for each of the acquired b-values (with the exception of the last one), the signal pattern into two compartments. An optimal distinction between the two compartments is assigned to the fit corresponding to the lowest sum of squared residuals.

After estimation of the diffusion tensor projections, the diffusion tensor was computed as reported by Hasan et al. (13).

For each framework, the fractional anisotropy,

$$FA = \sqrt{\frac{3}{2}\frac{(\lambda_{MAX} - MD)^2 + (\lambda_{MED} - MD)^2 + (\lambda_{MIN} - MD)^2}{\lambda_{MAX}^2 + \lambda_{MED}^2 + \lambda_{MIN}^2}} \quad [3]$$

and the mean diffusivity

$$MD = \frac{\lambda_{MAX} + \lambda_{MED} + \lambda_{MIN}}{3} \quad [4]$$

were computed from the three eigenvalues of the tensor (λ_{MAX}, λ_{MED}, λ_{MIN}) as a measure of the tensor's metrics.

ROIs were manually drawn around the right anterior and right posterior horn of the lateral ventricle, the anterior and posterior corpus callosum on the b0 image, and around the left nucleus caudatus and the left putamen on the respective coregistered T1-weighted slice of the study participant (Figure 1).

2.4 Statistical analysis

Statistical analysis was done using SPSS (IBM SPSS Statistics 25, Armonk, USA). Descriptive statistics were used to calculate the mean, standard deviation (SD), median and range of FA and MD for the different methods. The relative change of median FA and MD compared to the biexponential fitting was calculated as delta (Δ) and indicated in percentage change. The root mean square error

(rmse) was computed for each fitting model as a measure of the prediction accuracy according to the equation:

$rmse = \sum_i^n (y_i - \widehat{y_i})^2 / v$,

with y_i indicating the experimental points, $\widehat{y_i}$ referring to the predicted values and v being the difference between the number of data points *n* and the number of estimated parameters.

Friedman test was applied for testing of statistical significance in FA and MD between the two b-values, mono- and biexponential fit in the ROIs mentioned before. Significance values were adjusted by Bonferroni correction for multiple testing. Mann-Whitney U test was performed to evaluate for significant differences in FA and MD between the anterior and posterior part of the lateral ventricle and the corpus callosum, respectively, and between the nucleus caudatus and the putamen. A p-value of <0.05 was considered as statistically significant.

3. Results

MRI sessions were well tolerated by all subjects. Image quality also allowed the assessment of the diffusion properties in all volunteers.

An example of plots showing the raw data from different ROIs and fits using different methods is shown in Figure 2. In the nucleus caudatus, the IVIM model provided fit performance (rmse biexponentional fit: 2.42; rmse monoexponential: 5.54; rmse 2 b-values: 4.00). In the corpus callosum, the monoexponential model showed lower performance with an rmse of 5.23, while the IVIM model and the 2 b-values approaches performed similarly (rmse biexponential: 3.70; rmse 2 b-values: 2.14).The results are in line with the findings of the study on the larger cohort. In the nucleus caudatus, the proximity to the lateral ventricles suggests the potential contribution of the CSF motion on the quantification of the diffusion properties. No determinant influence of the fast-diffusion regime on the estimation of the diffusion properties was found for the corpus callosum.

3.1 Fractional anisotropy

The accounting for the fast diffusion compartments led to an increase of the median FA in most of the examined areas (Figure 3). When comparing the two b-value method, mono- and biexponential fit, there was a significant difference for the putamen (p=0.015) and the nucleus caudatus (p=0.022), with higher median FA when using the biexponential fit, and a trend towards statistical significance for the anterior horn of the lateral ventricle (p=0.074) (Table 2).

A certain dependency of the FA from the area of interest was found within the WM regions. The fractional anisotropy was highest for the anterior and posterior corpus callosum (Figure 3). The respective median values were in the range of 0.51 – 0.52 for the anterior and 0.45 – 0.47 for the posterior corpus callosum, depending on the calculation method (Table 1). Despite higher values for the anterior than the posterior corpus callosum, no significant difference could be detected ($p>0.5$ for all calculation methods).

The lowest FA was observed in the anterior and posterior horn of the lateral ventricle with median values between 0.04 – 0.06 and 0.08 – 0.10, respectively (Figure 3, Table 1), with no significant difference between these two regions ($p>0.1$ for all calculation methods).

Values for the median FA of the nucleus caudatus and putamen were in the range of 0.09 – 0.15 and 0.16 – 0.19 and did not significantly differ from each other ($p>0.1$ for all calculation methods).

3.2 Mean diffusivity

There was a significant difference between the different methods in nearly all examined regions: the anterior ($p=0.007$) and posterior horn of the lateral ventricle ($p=0.007$), the nucleus caudatus ($p=0.007$), putamen ($p=0.015$) and anterior corpus callosum ($p=0.015$) (Table 4). These differences were still significant when comparing the mono- with the biexponential fit, but not when comparing the two b-value method with the mono- or biexponential fit (Table 4).

Median values for the mean diffusivity were highest in the posterior horn of the lateral ventricle, followed by the anterior horn, nucleus caudatus and anterior corpus callosum, posterior corpus callosum and putamen (Figure 3). Mean and median values are listed in Table 3 for mono- and biexponential fit and the correction method.

The fraction of pseudo diffusion, averaged over the 20 diffusion-encoding directions, was higher in the lateral ventricle (anterior: 0.16±0.07; posterior: 0.21±0.09). Lower values were computed over the corpus callosum (anterior: 0.04±0.01; posterior: 0.06±0.04), the nucleus caudatus (0.07±0.02) and the putamen (0.06±0.02).

4. Discussion

Incoherent intravoxel fluid motion affects the evaluation of the diffusion properties in the static tissue and liquor (6, 7, 14). In this paper, we evaluated the potential detrimental effect of those movements on the evaluation of the diffusion tensor metric by comparing common approaches for DTI computation (such as two b-value based diffusion coefficient estimation, and monoexponential fit of

multiple b-values) to an IVIM-based approach, which corrects for the fast diffusion compartments before computation of the tensor. The fast diffusion components thereby not only include the effect of perfusion but may originate from additional sources, including fast diffusion components of the CSF as well, and cover a wide spectrum of magnitude (e.g. due to capillary segments of different size), which still may contaminate the signal sampled at higher b-values. For this reason we applied the method of Wurnig et al. (12) in our IVIM-based approach, which adjusts the separation of fast vs. slow dynamics pixel-wise.

For both, the MD and the FA, we found a dependency from the processing model. The accounting for the fast diffusion compartment led to a significant decrease of the MD in nearly all examined areas. For the FA, the correction depended on the observed region.

A dependency of the median FA from the calculation method can be expected in regions where a pseudo-diffusion component originated by the blood perfusion or by the CSF motion exists. This is most pronounced in regions containing larger vessels in the brain, or in areas next to the ventricles or the cerebral sulci, the latter especially in case of brain atrophy. In our study, we could show statistically significant differences in the FA of the nucleus caudatus depending on the method used in the tensor's elements estimation. The proximity to the lateral ventricles suggests the potential contribution of the CSF motion on the diffusion estimation of the nucleus caudatus. The correction for the fast-diffusion component led in this area to a significant increase in the fractional anisotropy. The putamen also revealed an equivalent trend in the FA. In the case of cardiac-gated brain DWI, IVIM measurements may even follow the CSF dynamic (7). In the current study, however, the metric of the diffusion tensor was measured over ROIs and DWI was performed without cardiac gating. Both factors suggest that the residual fast diffusion dynamic contamination in the nucleus caudatus and in the putamen should be isotropic. Therefore, the significant increase in FA measured in the nucleus caudatus and in the putamen after IVIM correction could be attributed to the mitigation of the isotropic contamination of the fast diffusion component.

No determinant influence of the fast-diffusion regime on the estimation of the diffusion properties was found for the corpus callosum. Similarly, no significant difference was found for the lateral ventricle when comparing the standard two-b-value method with the biexponential fit or all three methods against each other. Only the anterior horn of the lateral ventricle revealed a significant difference when using the mono- instead of the biexponential fit. This is in line with the results of Horie et al., which

detected irregularities of the CSF motion in the anterior horn of the lateral ventricle due to the link to the third ventricle via the foramen of Monro (15).

For the mean diffusivity, we found significant differences in nearly all examined regions, with the exception of the posterior corpus callosum, which was only significantly different between the two b-value method and the biexponential fit. The highest values for the mean diffusivity were found when calculating with the monoexponential fit, followed by the two b-value method. As expected, the lowest mean diffusivity was calculated when using the biexponential fit.

Concerning the dependency of the diffusion tensor's metric from the anatomical location, our results are in line with the literature. As expected, we found the highest FA in the corpus callosum, consisting of transverse fibers which connect the two brain hemispheres, with mean values in the range of 0.4 – 0.5. Slightly higher values for the FA were reported in the literature for this area with mean values for the genu corporis callosi of around 0.55 and for the splenium between 0.6 – 0.7 reported by Hasan et al. and Pfefferbaum et al. (16, 17) and around 0.7 - 0.8 described by Kochunov et al. (18) and Osuka et al. (19). For adolescents, Schneider et al. calculated values of around 0.7 for the genu corporis callosi. The lower anisotropy values found in this study could be attributed to the age-dependency of the FA. The lowest fractional anisotropy was calculated for the ventricles with mean values between 0.05 – 0.10, as expected for free fluid diffusion. In accordance with that, Hasan et al. (20) reported similar values for the fractional anisotropy of the lateral ventricle in 105 healthy volunteers of 0.09. Becker et al. recently showed a dependency of the fast-diffusion compartment in the ventricles from the diffusion-encoding direction, with a more than two-fold higher velocity in the anteroposterior direction than in craniocaudal and lateral direction (7). These results may explain the dependency of the MD value over the ventricle from the method used for the computation of the tensor's elements. In the gray matter areas (putamen and nucleus caudatus) we measured a mean FA of 0.1 – 0.2, which is in accordance with the literature (19, 21, 22).

The highest values for the mean diffusivity were found for the ventricles, with significantly higher values for the posterior horn than the anterior horn in the two b-value method and the monoexponential fit. This confirms again the importance of the fast-diffusion compartment in the ventricles. Similar results have been reported by Hasan et al. with a mean diffusivity of 2.8 10^{-3} mm^2/s (20).

Lower mean diffusivity was exhibited in the nucleus caudatus, corpus callosum, and putamen, with mean values all in the range of 0.5 – 1.0 10^{-3} mm^2/s. Hasan et al. reported similar results for the

nucleus caudatus in healthy volunteers of 0.7 10^{-3} mm^2/s. Compared to the corpus callosum and the nucleus caudatus, both lying next to the ventricles, the putamen showed the lowest mean diffusivity, probably due to minor partial volume contamination of the CSF. No significant difference was found between the mean diffusivity of the anterior and posterior corpus callosum for all three calculation methods ($p>0.09$), although higher values could be found for the anterior part. This is in accordance with the assumption described above that the CSF could have a dependency through a partial volume effect, which is more apparent for lower structures (11).

As limitation, it has to be mentioned that our study population consists of relatively young participants with a mean age of 36 years. Other publications reported an age-dependency in DTI with higher values in older people and more pronounced CSF contamination due to brain atrophy for the white matter. Nevertheless, as the focus lies on the comparison of the different methods, differences in the exact values of FA and MD are of minor relevance. Other values like the axial or radial diffusivity were not included in our calculation, but are also less used in the clinical routine. Assuming that the isotropic contamination of the fast IVIM component may be responsible for the significant lower FA measured in the nucleus caudatus and in the putamen using the monoexponential signal modelling. Removing the isotropic component would presumably lead to a reduction in the radial diffusivity (analogously to the effect on MD) and to an increase in AD (following the trend of the FA index).

5. Conclusions

We could show a significant dependency of the main elements of the diffusion tensor metrics from the methods used for the assessment of the projections of the diffusion tensor along the diffusion-encoding direction in the brain. The IVIM-based method proposed in this study allows for the correction of fast pseudo-diffusion contaminations, mainly attributable to CSF partial volume or to blood perfusion. The acquisition of more b-values for the subsequent correction of the fast diffusion compartments, as suggested in this study, results in longer acquisition times (approximately 30 minutes) as compared to the standard protocols. It has to be noted, that our MR protocol was designed for robust IVIM measurements without optimization regarding the acquisition time. Fewer b-values or the use of a multi-band sequence could potentially lead to even shorter acquisition times without compromising the quality of the results (23). Additionally, the IVIM-based method allows for a more accurate assessment of true diffusion quantities and for the estimation of the fast-diffusion compartments, which may have a clinical relevance. Compared to methods with FLAIR preparation,

the biexponential fit for DTI is expected to result in higher signal-to-noise ratio, which makes it an appropriate alternative to reduce signal contamination in DTI through CSF.

Acknowledgement: We thank Prof. Gustav Andreisek for his support with the local ethical committee application.

Funding: This work was supported by the Clinical Priority Program (KFSP) Molecular Imaging Network Zurich (minz) of the University of Zurich.

References

1. Drake-Perez M, Boto J, Fitsiori A, et al. Clinical applications of diffusion weighted imaging in neuroradiology. Insights Imaging. 2018.
2. Schaefer PW, Copen WA, Lev MH, Gonzalez RG**.** Diffusion-weighted imaging in acute stroke. Neuroimaging Clin N Am. 2005;15(3):503-30, ix-x.
3. Surov A, Meyer HJ, Wienke A**.** Correlation between apparent diffusion coefficient (ADC) and cellularity is different in several tumors: a meta-analysis. Oncotarget. 2017;8(35):59492-9.
4. Reddy JS, Mishra AM, Behari S, et al. The role of diffusion-weighted imaging in the differential diagnosis of intracranial cystic mass lesions: a report of 147 lesions. Surg Neurol. 2006;66(3):246-50; discussion 50-1.
5. Goveas J, O'Dwyer L, Mascalchi M, et al. Diffusion-MRI in neurodegenerative disorders. Magn Reson Imaging. 2015;33(7):853-76.
6. Le Bihan D, Breton E, Lallemand D, et al. Separation of diffusion and perfusion in intravoxel incoherent motion MR imaging. Radiology. 1988;168(2):497-505.
7. Becker AS, Boss A, Klarhoefer M, et al. Investigation of the pulsatility of cerebrospinal fluid using cardiac-gated Intravoxel Incoherent Motion imaging. Neuroimage. 2018;169:126-33.
8. Salminen LE, Conturo TE, Bolzenius JD, et al. Reducing Csf Partial Volume Effects to Enhance Diffusion Tensor Imaging Metrics of Brain Microstructure. Technol Innov. 2016;18(1):5-20.
9. Hajnal JV, Bryant DJ, Kasuboski L, et al. Use of fluid attenuated inversion recovery (FLAIR) pulse sequences in MRI of the brain. J Comput Assist Tomogr. 1992;16(6):841-4.
10. Pasternak O, Sochen N, Gur Y, et al. Free water elimination and mapping from diffusion MRI. Magn Reson Med. 2009;62(3):717-30.
11. Metzler-Baddeley C, O'Sullivan MJ, Bells S, et al. How and how not to correct for CSF-contamination in diffusion MRI. Neuroimage. 2012;59(2):1394-403.
12. Wurnig MC, Donati OF, Ulbrich E, et al. Systematic analysis of the intravoxel incoherent motion threshold separating perfusion and diffusion effects: Proposal of a standardized algorithm. Magn Reson Med. 2015;74(5):1414-22.
13. Hasan KM, Parker DL, Alexander AL**.** Comparison of gradient encoding schemes for diffusion-tensor MRI. J Magn Reson Imaging. 2001;13(5):769-80.
14. Surer E, Rossi C, Becker AS, et al. Cardiac-gated intravoxel incoherent motion diffusion-weighted magnetic resonance imaging for the investigation of intracranial cerebrospinal fluid dynamics in the lateral ventricle: a feasibility study. Neuroradiology. 2018;60(4):413-9.
15. Horie T, Kajihara N, Matsumae M, et al. Magnetic Resonance Imaging Technique for Visualization of Irregular Cerebrospinal Fluid Motion in the Ventricular System and Subarachnoid Space. World Neurosurg. 2017;97:523-31.
16. Hasan KM, Gupta RK, Santos RM, et al. Diffusion tensor fractional anisotropy of the normal-appearing seven segments of the corpus callosum in healthy adults and relapsing-remitting multiple sclerosis patients. J Magn Reson Imaging. 2005;21(6):735-43.
17. Pfefferbaum A, Sullivan EV**.** Increased brain white matter diffusivity in normal adult aging: relationship to anisotropy and partial voluming. Magn Reson Med. 2003;49(5):953-61.
18. Kochunov P, Chiappelli J, Hong LE**.** Permeability-diffusivity modeling vs. fractional anisotropy on white matter integrity assessment and application in schizophrenia. Neuroimage Clin. 2013;3:18-26.
19. Osuka S, Matsushita A, Ishikawa E, et al. Elevated diffusion anisotropy in gray matter and the degree of brain compression. J Neurosurg. 2012;117(2):363-71.
20. Hasan KM, Moeller FG, Narayana PA**.** DTI-based segmentation and quantification of human brain lateral ventricular CSF volumetry and mean diffusivity: validation, age, gender effects and biophysical implications. Magn Reson Imaging. 2014;32(5):405-12.
21. Hannoun S, Durand-Dubief F, Confavreux C, et al. Diffusion tensor-MRI evidence for extra-axonal neuronal degeneration in caudate and thalamic nuclei of patients with multiple sclerosis. AJNR Am J Neuroradiol. 2012;33(7):1363-8.
22. Hasan KM, Halphen C, Kamali A, et al. Caudate nuclei volume, diffusion tensor metrics, and T(2) relaxation in healthy adults and relapsing-remitting multiple sclerosis patients: implications for understanding gray matter degeneration. J Magn Reson Imaging. 2009;29(1):70-7.

23. Attenberger UI, Runge VM, Stemmer A, et al. Diffusion weighted imaging: a comprehensive evaluation of a fast spin echo DWI sequence with BLADE (PROPELLER) k-space sampling at 3 T, using a 32-channel head coil in acute brain ischemia. Invest Radiol. 2009;44(10):656-61.

Figures

Figure 1

A representative example of the ROI locations on slice MNI z=12. In pink and green the anterior and posterior horn of the lateral ventricle, in dark-blue and cyan the anterior and posterior part of the corpus callosum, in yellow the nucleus caudatus and in red the putamen are delineated.

Figure 2

Example of the DWI signal measured along a single diffusion encoding direction over the segmented anterior corpus callosum and the nucleus caudatus in one subject. Curves fitting the experimental data, and derived using the three fitting routines, were superimposed on the experimental data to allow visual inspection of the algorithm performances.

Figure 3

Box-Whisker plots showing the fractional anisotropy (A) and mean diffusivity (B) in different regions of the brain, calculated by two b-values, mono- and biexponential fit. The biexponential fit led to an increase of the median FA in nearly all examined areas and to a decrease of the median MD in all examined areas. The highest FA and MD were found for the corpus callosum and the lateral ventricle, respectively.

Tables

Table 1

Values for fractional anisotropy in different regions of interest in the brain analyzed with the two b-value method (2b), mono- (mono) and biexponential (bi) fit. Delta displays the difference related to the biexponential fit.

ROI	Parameter	Two b-values	Δ_{2b}	Mono-exponential fit	Δ_{mono}	Biexponential fit
Anterior corpus callosum	Mean / SD	0.46 / 0.10	-0.8%	0.46 / 0.10	+1.0%	0.47 / 0.09
	Median	0.52		0.51		0.52
	Range	0.30 – 0.54		0.30 – 0.54		0.33 – 0.55
Posterior corpus callosum	Mean / SD	0.40 / 0.14	-0.4%	0.41 / 0.15	-3.8%	0.41 / 0.14
	Median	0.45		0.47		0.45
	Range	0.16 – 0.53		0.17 – 0.57		0.19 – 0.54
Anterior horn of lateral ventricle	Mean / SD	0.05 / 0.01	+15.8%	0.05 / 0.01	+22.8%	0.06 / 0.01
	Median	0.05		0.04		0.06
	Range	0.04 – 0.07		0.04 – 0.06		0.04 – 0.08
Posterior horn of lateral ventricle	Mean / SD	0.08 / 0.03	+1.0%	0.08 / 0.03	+20.2%	0.09 / 0.04
	Median	0.10		0.08		0.10
	Range	0.04 – 0.11		0.04 – 0.10		0.04 – 0.13
Nucleus caudatus	Mean / SD	0.11 / 0.09	+39.3%	0.14 / 0.07	+14.7%	0.16 / 0.07
	Median	0.09		0.13		0.15
	Range	0.02 – 0.25		0.08 – 0.26		0.10 – 0.27
Putamen	Mean / SD	0.18 / 0.05	+3.1%	0.17 / 0.05	+17.3%	0.19 / 0.06
	Median	0.19		0.16		0.19
	Range	0.13 – 0.26		0.11 / 0.25		0.12 – 0.28

Table 2

P-values for differences between the various methods calculating the fractional anisotropy. Significant differences are highlighted in gray.

	Friedman	2b vs mono	2b vs bi	mono vs bi
Anterior Corpus callosum	0.165	-	-	-
Posterior Corpus callosum	0.247	-	-	-
Anterior horn of lateral ventricle	0.074	-	-	-
Posterior horn of lateral ventricle	0.247	-	-	-
Nucleus caudatus	0.022	1.000	0.034	0.081
Putamen	0.015	0.173	0.013	1.000

2b: Two b-value method, bi: biexponential fit, mono: monoexponential fit.

Table 3

Values for mean diffusivity (in units of 10^{-3} mm^2/s) in different regions of interest in the brain analyzed with the two b-value method (2b), mono- (mono) and biexponential (bi) fit. Delta displays the difference related to the biexponential fit.

ROI	Parameter	Two b-values	Δ_{2b}	Mono-exponential fit	Δ_{mono}	Biexponential fit
Anterior corpus callosum	Mean / SD	0.91 / 0.13		0.93 / 0.13		0.85 / 0.12
	Median	0.96	-3.2%	0.97	-4.8%	0.93
	Range	0.76 – 1.03		0.77 – 1.06		0.72 – 0.96
Posterior corpus callosum	Mean / SD	0.79 / 0.09		0.80 / 0.11		0.72 / 0.08
	Median	0.80	-12.6%	0.84	-18.22%	0.71
	Range	0.69 – 0.89		0.65 – 0.93		0.65 – 0.82
Anterior horn of lateral ventricle	Mean / SD	2.20 / 0.13		2.30 / 0.13		2.09 / 0.14
	Median	2.23	-9.4%	2.28	-11.5%	2.04
	Range	2.05 – 2.38		2.14 – 2.47		1.92 – 2.27
Posterior horn of lateral ventricle	Mean / SD	2.63 / 0.25		2.70 / 0.25		2.49 / 0.37
	Median	2.60	-5.5%	2.75	-11.7%	2.47
	Range	2.31 – 2.91		2.38 – 2.94		1.97 – 2.88
Nucleus caudatus	Mean / SD	0.99 / 0.25		1.02 / 0.23		0.86 / 0.18
	Median	0.95	-11.2%	0.98	-14.4%	0.86
	Range	0.73 – 1.36		0.75 – 1.36		0.65 – 1.13
Putamen	Mean / SD	0.72 / 0.05		0.75 / 0.07		0.71 / 0.05
	Median	0.73	-0.8%	0.77	-6.5%	0.72
	Range	0.67 – 0.79		0.67 – 0.82		0.66 – 0.79

Table 4

P-values for differences between the various methods calculating the mean diffusivity. Significant differences are highlighted in gray.

	Friedman	2b vs bi	mono vs bi	2b vs mono
Anterior Corpus callosum	0.015	0.173	0.013	1.000
Posterior Corpus callosum	0.074	-	-	-
Anterior horn of lateral ventricle	0.007	0.342	0.005	0.342
Posterior horn of lateral ventricle	0.007	0.342	0.005	0.342
N. caudatus	0.007	0.342	0.005	0.342
Putamen	0.015	0.173	0.013	1.000

2b: Two b-value method, bi: biexponential fit, mono: monoexponential fit.

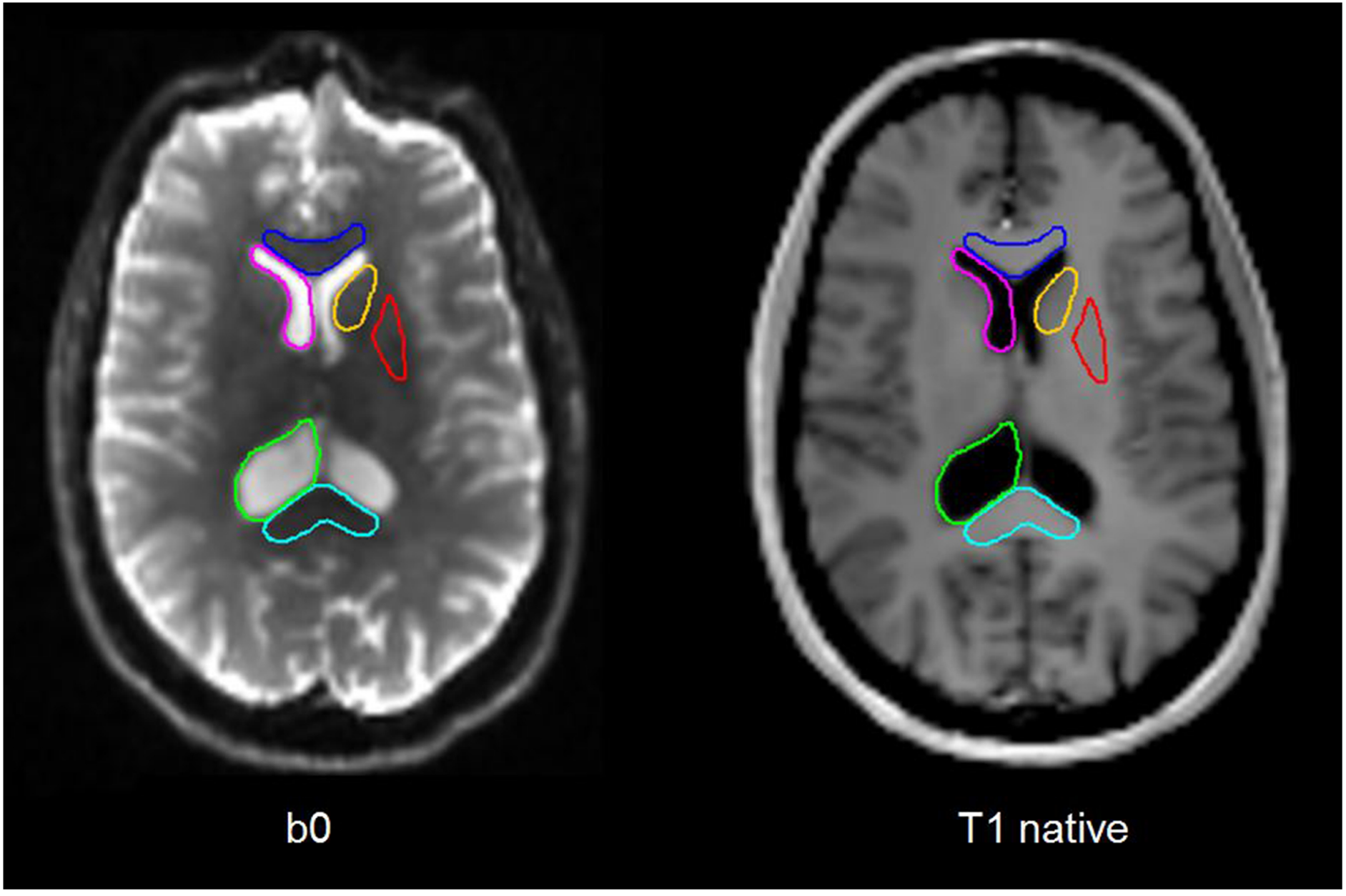

Figure 1

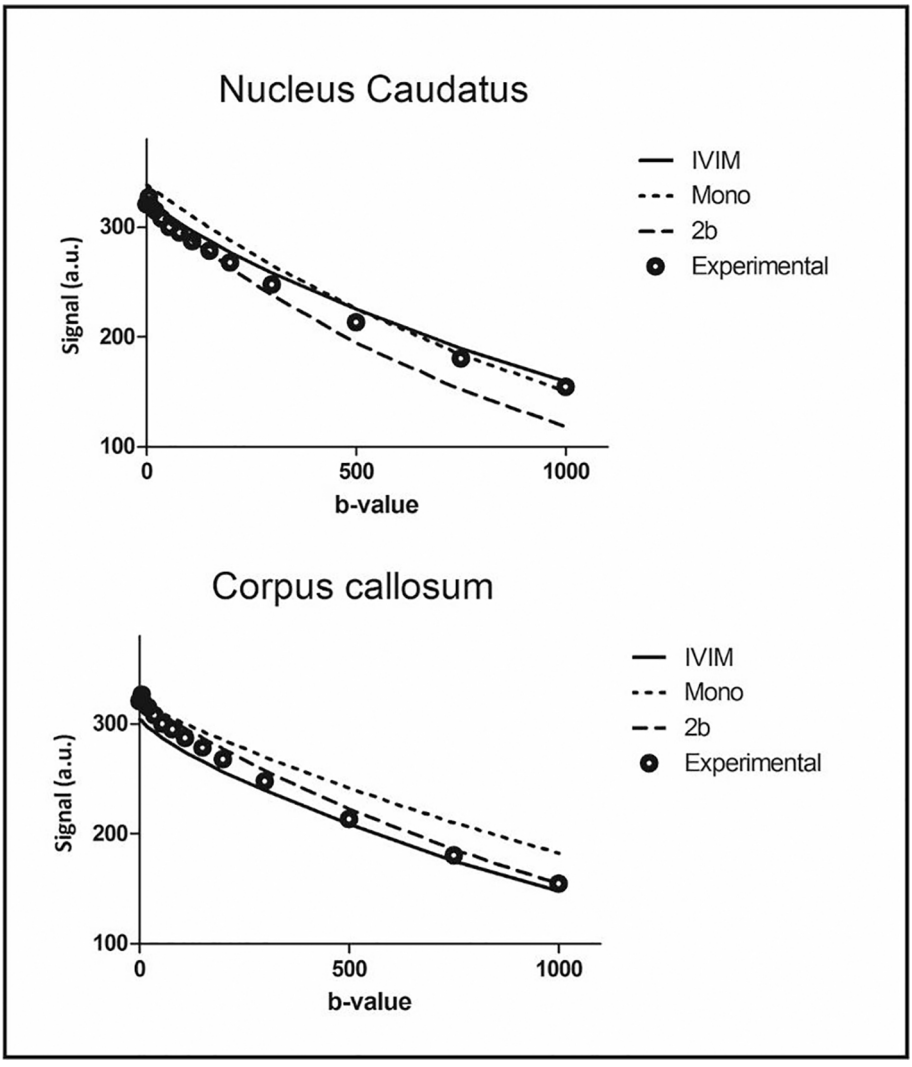
Nucleus Caudatus
IVIM
Mono
2b
Experimental
Signal (a.u.)
300
200
100
0
500
1000
b-value
Corpus callosum
IVIM
Mono
2b
Experimental
Signal (a.u.)
300
200
100
0
500
1000
b-value

Figure 2

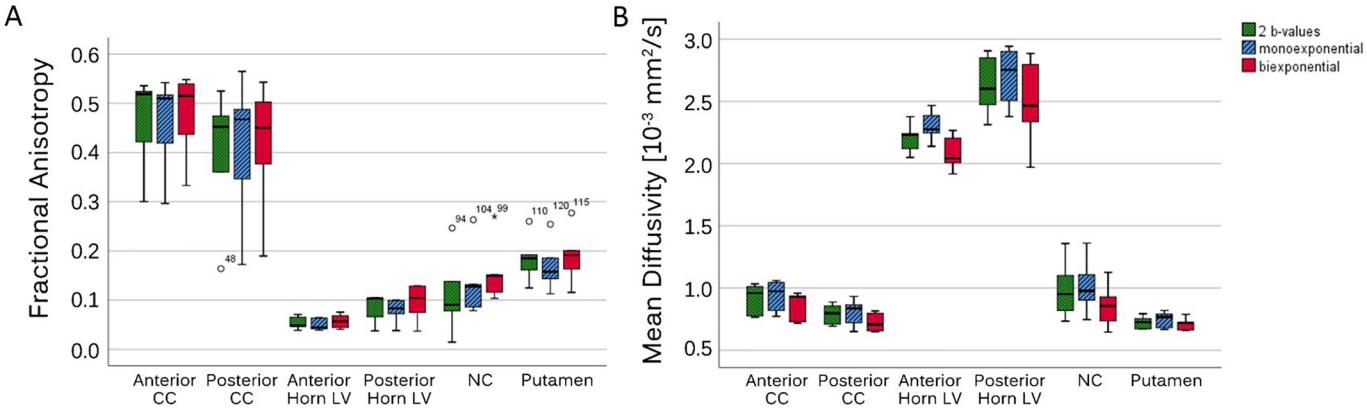
A
Fractional Anisotropy
0.6
0.5
0.4
0.3
0.2
0.1
0.0
48
94
104
99
110
120
115
Anterior CC
Posterior CC
Anterior Horn LV
Posterior Horn LV
NC
Putamen
B
Mean Diffusivity [10-3 mm2/s]
3.0
2.5
2.0
1.5
1.0
0.5
2 b-values
monoexponential
biexponential
Anterior CC
Posterior CC
Anterior Horn LV
Posterior Horn LV
NC
Putamen

Figure 3